Langmuir

ARTICLE

pubs.acs.org/Langmuir

Formation of Kinetically Trapped Nanoscopic Unilamellar Vesicles from Metastable Nanodiscs

Mu-Ping Nieh,[*,†] Paul Dolinar,[‡] Norbert Kučerka,[§,∥] Steven R. Kline,[⊥] Lisa M. Debeer-Schmitt,[#] Kenneth C. Littrell,[#] and John Katsaras[§,#,□,△]

[†]Department of Chemical, Materials & Biomolecular Engineering, Institute of Materials Science, University of Connecticut, Storrs, Connecticut 06269, United States

[‡]University of Ottawa, Ottawa, Ontario, K1N 6N5, Canada

[§]Canadian Neutron Beam Centre, Chalk River Laboratories, National Research Council, Chalk River, Ontario, K0J 1J0, Canada

[∥]Department of Physical Chemistry of Drugs, Comenius University, 835 35 Bratislava, Slovakia

[⊥]National Institute of Standards and Technology, Gaithersburg, Maryland 20899, United States

[#]Neutron Scattering Science Division, Oak Ridge National Laboratory, Oak Ridge, Tennessee 37831-6393, United States

[□]Department of Physics, Brock University, St. Catharines, Ontario, L2S 3A1, Canada

[△]Guelph-Waterloo Physics Institute and Biophysics Interdepartmental Group, University of Guelph, Guelph, Onatrio, N1G 2W1, Canada

Supporting Information

ABSTRACT: Zwitterionic long-chain lipids (e.g., dimyristoyl phosphatidylcholine, DMPC) spontaneously form onion-like, thermodynamically stable structures in aqueous solutions (commonly known as multilamellar vesicles, or MLVs). It has also been reported that the addition of zwitterionic short-chain (i.e., dihexanoyl phosphatidylcholine, DHPC) and charged long-chain (i.e., dimyristoyl phosphatidylglycerol, DMPG) lipids to zwitterionic long-chain lipid solutions results in the formation of unilamellar vesicles (ULVs). Here, we report a kinetic study on lipid mixtures composed of DMPC, DHPC, and DMPG. Two membrane charge densities (i.e., [DMPG]/[DMPC] = 0.01 and 0.001) and two solution salinities (i.e., [NaCl] = 0 and 0.2 M) are investigated. Upon dilution of the high-concentration samples at 50 °C, thermodynamically stable MLVs are formed, in the case of both weakly charged and high salinity solution mixtures, implying that the electrostatic interactions between bilayers are insufficient to cause MLVs to unbind. Importantly, in the case of these samples small angle neutron scattering (SANS) data show that, initially, nanodiscs (also known as bicelles) or bilayered ribbons form at low temperatures (i.e., 10 °C), but transform into uniform size, nanoscopic ULVs after incubation at 10 °C for 20 h, indicating that the nanodisc is a metastable structure. The instability of nanodiscs may be attributed to low membrane rigidity due to a reduced charge density and high salinity. Moreover, the uniform-sized ULVs persist even after being heated to 50 °C, where thermodynamically stable MLVs are observed. This result clearly demonstrates that these ULVs are kinetically trapped, and that the mechanical properties (e.g., bending rigidity) of 10 °C nanodiscs favor the formation of nanoscopic ULVs over that of MLVs. From a practical point of view, this method of forming uniform-sized ULVs may lend itself to their mass production, thus making them economically feasible for medical applications that depend on monodisperse lipid-based systems for therapeutic and diagnostic purposes.

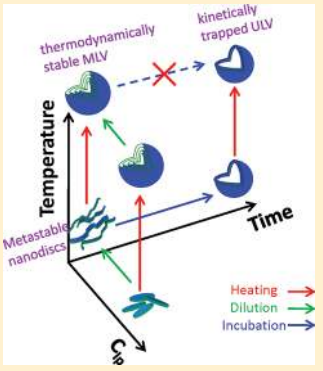

INTRODUCTION

Because of their biocompatibility, stability, and capability for controlled release of encapsulated materials, liposomes composed of phospholipids have great potential as *in vivo* delivery carriers. However, the lamellarity of liposomes is an important parameter that dictates their loading capacity and *in vivo* circulation half-life. Generally speaking, long-chain zwitterionic lipids [e.g., phosphatidylcholines (PCs) with hydrocarbon chains of ≥12] form multilamellar vesicles (MLVs) in aqueous solutions. These MLVs have an intrinsically lower payload capacity and a greater probability of being taken up by the reticuloendothelial system—presumably because of their large size (on the order of micrometers).[1,2] Thermodynamically, it is possible to unbind the interacting bilayers making up MLVs, thus forming pauci-lamellar vesicles or unilamellar vesicles (ULVs). MLV unbinding has been studied theoretically[3−6] and demonstrated experimentally.[7,8] In short, as the undulation and Coulombic repulsive forces (e.g., in systems with sufficient amounts of charged lipids) begin to dominate over the van der Waals attraction force, the lamellar repeat spacing, *d*, of MLVs increases with increasing

Received: June 21, 2011
Revised: September 27, 2011
Published: September 27, 2011

ACS Publications © 2011 American Chemical Society

dx.doi.org/10.1021/la2023314 | *Langmuir* 2011, 27, 14308–14316

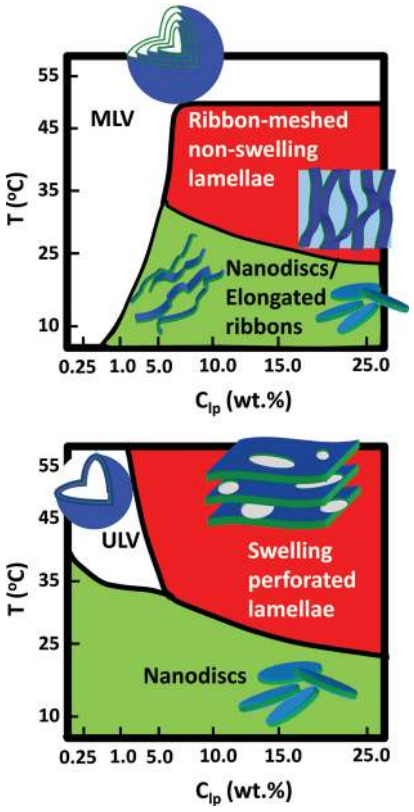

Figure 1. Aggregate structures formed by (a) a zwitterionic phospholipid mixture ([DMPC]/[DHPC] = 3.2), and (b) a charged phospholipid mixture ([DMPC]/[DHPC] = 3.2 and [DMPG]/[DMPC] = 0.01) over a range of temperatures and total lipid concentrations.

water content (i.e., decreased lipid concentration), until such a point that the lamellae unbind from each other resulting in the formation of ULVs. This thermodynamically driven transformation from MLVs to ULVs does not involve other intermediate morphologies. However, in the case of zwitterionic lipid bilayers, such morphological transformations are not observed, as MLVs will only swell up to some limiting value of d whereupon any further addition of water has no effect on them [e.g., dimyristoyl (DMPC) and dipalmitoyl (DPPC) PC bilayers].

A different approach of forming ULVs from MLVs involves the addition of short-chain lipids or surfactants.[9−11] In the case of lipid mixtures containing long- and short-chain lipids, bilayered nanodiscs (commonly referred to as bicelles) are observed when the long-chain lipid is in the gel phase and the short-chain lipid is in the L_α or liquid crystalline phase.[12,13] In this case, the two lipids are segregated, whereby the disc's planar bilayer is composed of the long-chain lipid and the disc's highly curved edge is occupied by the short-chain lipid, thus decreasing the system's free energy.[14−26] Recently, in the case of the zwitterionic long- and short-chain lipids, DMPC and dihexanoyl PC (DHPC), respectively, cryogenic transmission electron microscopy (cryo-TEM)[27] and small angle neutron scattering (SANS) data[12,13,28] have yielded similar structural phase diagrams. Presently, the general consensus regarding the aggregate structures of these lipids, as a function of lipid concentration (C_{lp}) and temperature, is summarized in Figure 1a.[13,28] For example, nanodiscs and/or bilayered ribbons are found at low and intermediate temperatures, respectively, while at high temperatures (above the melting transition temperature of DMPC, T_M), perforated lamellae (or MLVs) and liposomes (MLVs and ULVs) are observed at high and low C_{lp}, respectively—presumably due to increased miscibility between DMPC and DHPC.[12,13,27−30] Over the past decade, these mixtures have been extensively studied mainly because of their ability, in magnetic fields, to align membrane-associated proteins in their bioactive conformations, as has been demonstrated by numerous nuclear magnetic resonance (NMR) studies, for example.[31−44]

In order to obtain uniform-sized nanoscopic ULVs from a mixture of short- and long-chain phospholipids, a small amount of the long-chain charged lipid (∼0.01 mol fraction of total long-chain lipids), dimyristoyl phosphatidylglycerol (DMPG), is needed.[28,45−47] Since these ULVs self-assembled via different pathways, they were considered to be thermodynamically stable.[48] However, their size and polydispersity can vary extensively, depending on their path of formation. The structural phase diagram of a lipid mixture doped with DMPG has been established with SANS (Figure 1b).[13,28] Comparison of the structural phase diagrams with and without DMPG (Figure 1a,b) clearly shows that the addition of the charged lipid causes MLVs to break up into ULVs. This observation is consistent with theory,[3−5] which suggests that the Coulombic repulsion between membranes dominates as a result of the increased charge density imparted by DMPG. The structural transformation from cylindrical micelles to ULVs (observed in a mixture of lecithin and bile salt) has also been reported, whereby the resultant ULV morphology was found to be dependent on system kinetics, and not thermodynamics.[49,50] Another distinct difference between the two structural phase diagrams shown in Figure 1a,b is the significant upward shift in temperature of the boundary separating vesicles from nanodiscs at low C_{lp}, which until now has not been well-understood.

We report a SANS study on how lipid aggregate morphology is affected by charge density (i.e., DMPG content) and salt concentration, as well as the system's kinetic pathway of formation. The main results of this study are as follows: (a) the formation of nanoscopic ULVs (i.e., disc-to-vesicle transition) in a nominally thermodynamically stable MLV system; this method of ULV formation can be used to mass produce them, eliminating many of the inherent problems associated with extrusion and sonication protocols; (b) until now, the upward shift in temperature observed in the disc-to-vesicle transition when a charged lipid was introduced to a zwitterionic "bicelle" lipid mixture (Figure 1) has remained unclear. The present data imply that this shift in temperature may be attributed to the instability of nanodiscs at low temperature (low-T).

MATERIALS AND METHODS

Phospholipids (DMPC, DHPC, and DMPG) were purchased from Avanti Polar Lipids and used as received. NaCl (≥99.5%) was purchased from Sigma-Aldrich Co. and dissolved in D_2O to produce a 0.2 M solution. Three series of samples with a constant molar ratio of long-chain to short-chain lipid, Q (i.e., ([DMPC]+[DMPG])/[DHPC]) = 4 and a C_{lp} = 10% (mass fraction) were prepared in D_2O as follows: (1) [DMPG]/[DMPC] (denoted as R) = 0.01 (control sample); (2) R = 0.001; and (3) R = 0.01, [NaCl] = 0.2 M. The required amount of lipids was first weighed according to the molar ratio and thoroughly mixed (by vortexing and temperature cycling between 4 and 50 °C) in either pure D_2O or 0.2 M NaCl D_2O buffer until the solutions were completely transparent at low-T, ensuring a homogeneous dispersion of the samples. C_{lp} = 10% samples were then further diluted through a number of intermediate concentrations with either D_2O or a 0.2 M NaCl D_2O

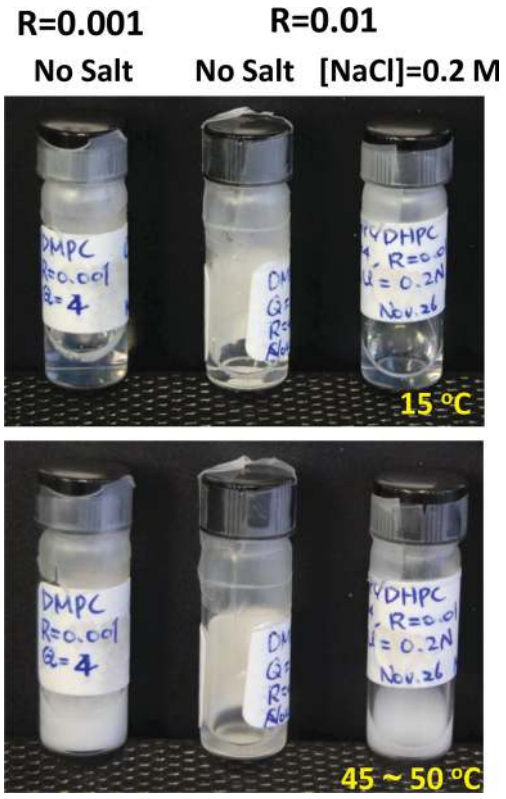

Figure 2. Appearance of three samples at a C_{lp} of 10% (Q = 4): R = 0.001 with no salt (left), R = 0.01 with no salt (middle), and R = 0.01 with [NaCl] = 0.2 M (right) at 15 °C (top), and between 45 and 50 °C (bottom). Transparent samples (15 °C) are made up of small aggregates, which are shown by SANS to be nanodiscs (dilute samples). The translucent, gel-like (R = 0.01) and opaque samples (R = 0.001 and R = 0.001, [NaCl] = 0.2 M) are made up of extended lamellae and MLVs, respectively (also confirmed by SANS measurements in Figure 3).

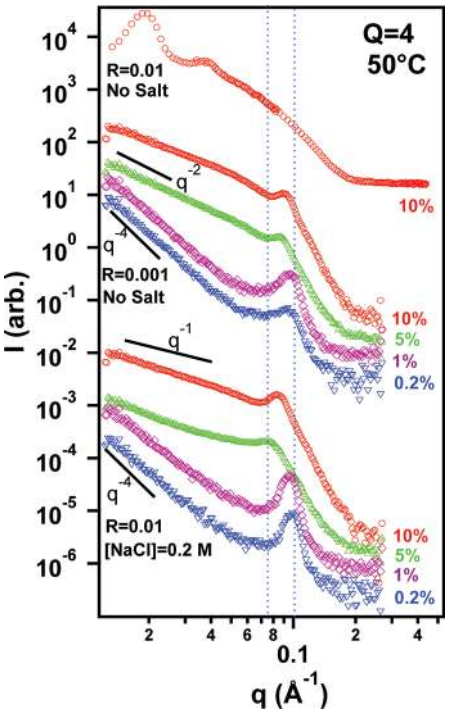

Figure 3. SANS data of C_{lp} = 10% Q = 4 samples undergoing high-T dilution and measured at 50 °C. The control sample (R = 0.01, top circles) has a scattering pattern characteristic of lamellae that are capable of swelling. The other samples (R = 0.001 no salt and R = 0.01 with [NaCl] = 0.2 M) with C_{lp} = 10% (circles), 5% (top-pointed triangles), 1% (diamonds), and 0.2% (bottom-pointed triangles) show a nonswelling lamellar phase, namely, MLVs either with an insufficient charge density or where their charges have been screened. Error bars (one standard deviation) for all SANS data are generally within the size of the symbols, except at q > 0.1 Å^{-1}, where their size is comparable to the scatter in the data.

solution, always maintaining the same salinity as the initial 10% samples. Dilutions at both high (i.e., 50 °C) and low (i.e., 4 °C) temperatures were performed on various samples, and SANS measurements were taken at each condition within 1 h after sample preparation. SANS data of low-T diluted samples were also collected after the temperature was raised to 50 °C. Moreover, in order to gain insight into the stability of discoidal micelles, a SANS measurement was performed on a 0.3% (R = 0.001, no salt) sample after 20 h of incubation at 4 °C—to compare with those from the nonincubated samples.

SANS experiments were conducted at either the NG3-SANS instrument located at the NIST (National Institute of Standards and Technology) Center for Neutron Research (NCNR, Gaithersburg, Maryland, USA), or the CG2-SANS instrument located at the High Flux Isotope Reactor (HFIR, ORNL, Oak Ridge, Tennessee, USA). At the NG3-SANS, 6 Å wavelength (λ) neutrons with a $\Delta\lambda/\lambda$ = 15% were used in combination with sample-to-detector distances (SDD) of 13.17, 5, and 1.33 m, yielding a range of scattering vectors, $q = [(4\pi)/\lambda \sin(\theta/2)$, where θ is the scattering angle], from 0.0035 Å^{-1} to 0.4 Å^{-1}. At the CG2-SANS, 4.75 Å ($\Delta\lambda/\lambda$ = 15%) neutrons and two SDDs (i.e., 4 and 18.5 m) were used to cover a q range from 0.004 Å^{-1} to 0.26 Å^{-1}. All 2-D raw data were corrected for sample and empty cell transmission, as well as background scattering, and then reduced to 1-D intensity plots as a function of q. The spatial resolution of the SANS instruments used can be found in ref 51, and was calculated according to ref 52. SANS data were then fitted with the appropriate models (i.e., core−shell disc, cylinder with an elliptic cross-section, or spherical shell) that have been developed by NCNR using the software *IGOR-Pro*.[53] Detailed description of the models are presented in the Supporting Information. Fitting curves were "smeared" using the appropriate instrumental resolution. However, a structure factor (interparticle interaction) was not incorporated into the data analysis, as it is not necessary in the case of dilute samples—it should be noted that the data of nondilute samples were not fitted. As a result, a fewer number of parameters were needed to fit the SANS data.

RESULTS

Sample Appearance. The top panel in Figure 2 illustrates the appearance of all three 10% samples (R = 0.01, R = 0.001, and R = 0.01 with 0.2 M NaCl) at 15 °C. The fact that they are transparent and of low viscosity at such high C_{lp} implies the presence of small particles. After diluting the samples to <1% at low-T, all SANS data are consistent with the presence of discoidal micelles or ribbon-like aggregates (to be discussed in a later section)—structural phase diagrams (at low-T) shown in Figure 1. However, at elevated temperatures (e.g., between 45 and 50 °C), the R = 0.001 (no salt) and R = 0.01 (0.2 M NaCl) samples turned opaque, whereas the control sample (R = 0.01 with no salt) became viscous and slightly translucent. The visual properties of opaqueness and translucency indicate the presence of micrometer-size particles/aggregates. It should be noted that at this lipid concentration (i.e., C_{lp} = 10%) the appearances of all the

samples at a given temperature are reproducible, implying that the same morphologies are always observed. Similar phenomena are observed with C_{lp} samples >5%. However, the same structural transformations may not be reproducible with lower C_{lp} samples.[45,48]

High-T (50 °C) Dilution. SANS data of the 10% control sample (R = 0.01) at 50 °C exhibit distinct first- and second-order quasi-Bragg peaks (at q_o = 0.019 and 0.038 Å^{-1}, respectively) indicative of long-range, out-of-plane interactions with a lamellar repeat spacing, d, of 337 Å ($d = 2\pi/q_1$) (Figure 3). This lamellar spacing is similar to that of a DMPC/DHPC/DMPG mixture at the same C_{lp},[47] where perforated lamellae have been observed. These results are also consistent with the aforementioned translucent appearance and data from a previous cryo-TEM report.[54] The Coulombic repulsion induced from the presence of the charged DMPG (in the case of R = 0.01) is sufficient to unbind DMPC MLVs, as predicted by theory.[3−5] However, the SANS patterns of the two other C_{lp} = 10% lipid mixtures (i.e., R = 0.001 and R = 0.01, [NaCl] = 0.2 M) are drastically different from that of the control sample. For example, a sharp quasi-Bragg peak appears at q_o = 0.09 Å^{-1} and 0.085 Å^{-1} in R = 0.001 and R = 0.01, [NaCl] = 0.2 M samples, respectively, corresponding to repeat spacings of 69.8 and 73.9 Å, respectively. Diluting both samples to 5% (at 50 °C) only leads to a marginal swelling of the lamellae (74.0 and 82.5 Å, respectively), implying that either there is insufficient Coulombic repulsion (in the case of R = 0.001) or the charges are screened (in the case of R = 0.01, [NaCl] = 0.2 M), thus preventing the lamellae from freely swelling. (It should be noted that this result is also consistent with the observed opaqueness of the samples, i.e., the presence of large aggregates such as MLVs).

Although both systems exhibit a similar swelling behavior, their aggregate morphologies are most likely very different. For example, in the case of R = 0.001 samples (for both C_{lp} = 5% and 10%), the low-q scattered intensity follows a q^{-2} dependence, consistent with a planar structure, while in the case of R = 0.01, [NaCl] = 0.2 M samples (for both C_{lp} = 5% and 10%), the scattered intensity decays as q^{-1}, consistent with the presence of elongated aggregates.[55] The planar structure is best described by a lamellar morphology, while the elongated structure is most likely made up of entangled, ribbon-like lamellae,[28] or tubular/elongated vesicles similar to those reported in octyl glucoside/egg phosphatidylcholine[56] or DMPC/geraniol[57] mixtures. Diluting the sample further to 1% and 0.2% results in the lamellar repeat spacing quasi-Bragg peak shifting to higher q (~0.095 Å^{-1}), namely, a d of 66 Å for both R = 0.001 and R = 0.001, [NaCl] = 0.2 M samples. The fact that this spacing is in good agreement with that of liquid crystalline (L_α) DMPC MLVs[58−60] implies that both lipid mixtures form MLVs that are composed almost entirely of DMPC. Importantly, the Porod regime of these scattering curves exhibits a q^{-4} dependence, further proof of the presence of large aggregates, namely, MLVs. The resultant thermodynamically stable MLVs obtained from high-T dilution suggests that charge-reduced (R = 0.001) and salt-doped (R = 0.01, [NaCl] = 0.2 M) samples are in many ways similar to zwitterionic lipid systems (i.e., with no DMPG), as shown in Figure 1b. It should be noted that in all cases the SANS scattering observed is isotropic, indicative of randomly oriented aggregates on the macroscopic scale—even though the individual particles themselves may be anisotropic (i.e., ribbons, lamellae).

Low-T (10 °C) Phases Immediately after Dilution. Nanodiscs have been observed in amphiphilic mixtures[61] and are characterized by two distinct spontaneous curvatures. For example, in the case of lipid mixtures, the long-chain lipids form the disc's planar region and the short-chain lipids coat the disc's rim.[54,62] In the case of lipid/protein mixtures (e.g., membrane scaffold proteins like apolipoproteins), the protein sequesters into the disc's rim and the lipids form the bilayer.[63−67] Nanodiscs composed of two lipids (e.g., long- and short-chain lipids) are usually found at low-T, as shown in Figure 1. This is presumably due to the immiscibility between the gel long-chain lipid and the liquid crystalline short-chain lipid. Supporting this notion is a DSC study reporting that the T_M of DMPC is not strongly affected when incorporated with DHPC.[68] As such, nanodiscs are commonly thought to be thermodynamically stable at low temperatures.[48] However, to the best our knowledge a systematic study has yet to be conducted on the stability of DMPC/DHPC discoidal micelles (at low-T)—except for a few kinetic studies on the micelle-to-vesicle transition in egg lecithin/bile salt mixtures, where the transition was triggered by dilution.[49,50]

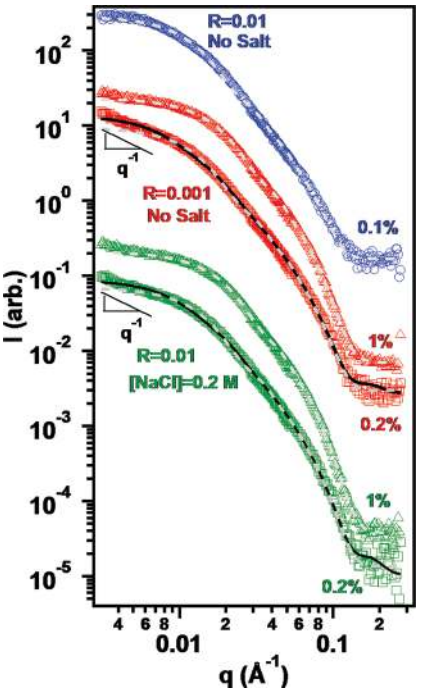

Figure 4. SANS data of Q = 4 samples diluted at 4 °C and measured less than 3 h after the sample was prepared. The 0.1% R = 0.01 (circles), 1.0% R = 0.001 (red triangles), and R = 0.01, [NaCl] = 0.2 M (green triangles) data are fitted reasonably well with the core−shell disc model (dashed curves). The 0.2% of R = 0.001 (red squares) and R = 0.01, [NaCl] = 0.2 M (green squares) data are fitted using both the core−shell disc model (dashed curves) and the elongated ellipsoidal model (solid curves).

Low-T (10 °C) SANS data from all three samples (R = 0.01, R = 0.001, and R = 0.01, [NaCl] = 0.2 M) at low lipid concentrations (≤1%)—used in order to minimize the possibility of interparticle interactions—are shown in Figure 4. It should be noted that all samples are diluted from the original 10% C_{lp} condition at low-T (4 °C) and studied at 10 °C immediately after dilution. SANS data of the control sample (C_{lp} = 0.1% and R = 0.01) are best fitted with the core−shell discoidal model (Supporting Information section I), where the core and shell represent the hydrophobic acyl chains and hydrophilic headgroups, respectively. During the fitting process, the shell and core thicknesses are constrained within the ranges 5−15 Å and

Table 1. Parameters Obtained from Best Fits to the Data Using Various Models (i.e., Core−Shell Disc, Cylinder with an Ellipsoidal Cross Section and Spherical Shell)

	core−shell disc			cylinder with an ellipsoidal cross section			spherical shell		
samples[a]	core radius (Å)	shell (Å)	core thickness (Å)	short-axis (Å)	long-axis (Å)	length (Å)	inner radius (Å)	shell (Å)	p^b
R = 0.01 C_{lp} = 0.1% 10 °C (*ap*)	186 ± 15	15 ± 1	34 ± 2						
R = 0.001 C_{lp} = 0.2% 10 °C (*ap*)	130 ± 12	15 ± 1	32 ± 2						
R = 0.01 [N] = 0.2 M C_{lp} = 1% 10 °C (*ap*)	123 ± 10	15 ± 1	34 ± 3						
R = 0.001 C_{lp} = 0.2% 10 °C (*ap*)				26 ± 4	130 ± 15	610 ± 25			
R = 0.001 [NaCl] = 0.2 M C_{lp} = 0.2% 10 °C (*ap*)				26 ± 4	130 ± 15	500 ± 20			
R = 0.001 C_{lp} = 0.3% 10 °C (*incub.*)							164 ± 9	37 ± 3	0.25
R = 0.001 C_{lp} = 0.3% 50 °C after 10 °C (*incub.*)							194 ± 15	32 ± 3	0.25

[a] *ap*, as prepared; *incub*, incubated. [b] *p*, polydispersity of vesicular radius.

30−40 Å, respectively—realistic values for a PC lipid bilayer. The best fits (dashed line) to the data result in a shell thickness of 15 ± 1 Å, a core thickness of 34 ± 2 Å, and a disc radius of 186 ± 15 Å. In the case of 1% C_{lp} samples with a reduced charged density (R = 0.001) and increased salinity (R = 0.01, [NaCl] = 0.2 M), an invariant shell thickness (15 Å) is obtained from the best fits to the SANS data, while the core thickness and disc radius are determined to be 32 ± 3 Å and 130 ± 12 Å, respectively, for the R = 0.001 sample, and 34 ± 3 Å and 123 ± 10 Å, respectively, for the R = 0.01, [NaCl] = 0.2 M sample. Compared to the R = 0.01 and C_{lp} = 0.1% sample, the smaller disc radii of these 1% samples are presumably due to more DHPC being available to stabilize the disc's rim. It should be noted that nanodiscs of similar dimensions (i.e., radius and thickness) have been repeatedly observed in DMPC/DMPG/DHPC mixtures at low-T.[12,13,45,48] The current best-fit core thickness is consistent with the literature value for the hydrophobic thickness of gel-phase DMPC bilayers obtained from X-ray diffraction (30 Å).[69] However, the shell thickness is slightly larger (by about 5 Å), possibly due to the high contrast offered by D_2O and the lack of a well-defined boundary between D_2O and the PC headgroups.

The simple disc model is, however, inadequate when it comes to fitting lower C_{lp} (i.e., 0.2%) data at low-q (i.e., <0.006 Å^{-1}), where large deviations are observed for both weakly charged (R = 0.001) and highly screened (R = 0.01, [NaCl] = 0.2 M) samples (Figure 4). The deviated low-q data reveal the onset of a q^{-1} dependence, a possible sign of elongated aggregates (presumably ribbon-like micelles). Although the range of q^{-1} dependence spans less than a decade (making it difficult to conclusively identify the presence of elongated objects), cryo-TEM studies have demonstrated the existence of elongated aggregates in a similar lipid mixture, at a similar temperature.[54] Moreover, the fact that these samples exhibit the same decay behavior as nanodiscs at higher q suggests that the elongated micelles have a thickness similar to that of nanodiscs.

On the basis of the above-mentioned evidence, we propose that the most likely structure for these samples (i.e., R = 0.001 and highly screened R = 0.01, [NaCl] = 0.2 M) is bilayered ribbons, which can be adequately described by a cylindrical model with an elliptical cross section (Supporting Information section II). The major and minor axes represent the width of the ribbon and the bilayer thickness, respectively. However, to minimize the number of fitting parameters, a few assumptions are made as follows: (1) the neutron scattering length density (SLD) of the ribbons is assumed to be uniform; (2) the ribbons are assumed to be rigid and their size is uniform. The first assumption is defensible due to the low contrast between the hydrophilic and the hydrophobic regions of the ribbon, compared to D_2O. The other assumption can, however, affect the best fits to the SANS data. The best fit values of the major and minor axes are 130 ± 15 Å and 26 ± 4 Å (for both samples), respectively. These values are consistent with the notion of the proposed ribbon model, where ribbon thickness (twice that of the minor axis, 52 ± 8 Å) agrees well with that obtained from the discoidal model [i.e., (15 Å + 34 Å) = 49 ± 3 Å], shown in Table 1. From the best fits, the length of these ribbons is determined to be about 610 Å for the charge-reduced sample and about 500 Å for the salt-added sample. It should be noted that during the fitting procedure this model did not constrain the major and minor axes, thus allowing for the emergence of other possible morphologies, e.g., cylindrical rods, oblate ellipsoids, or prolate ellipsoids. The best fit results from these data are listed in Table 1.

Although the above-mentioned model fits the SANS data reasonably well over most of the q range, the best fits do not adequately address the scattering data at low-q. For example, the approaching plateau region is not observed in the data as calculated by the model. This is unlikely the result of instrumental resolution—which has been accounted for when fitting the data—but is more likely due to nonuniform lengths of flexible ribbons (as discussed previously), features which are not accounted for in the present model, but have been previously observed in a similar system.[27,54] It should also be noted that the present observations do not exactly follow the structural phase diagram of a zwitterionic lipid mixture at low-T and low C_{lp} (Figure 1b), where MLVs are commonly observed. This would imply that the charged DMPG lipid, though present in only a small amount, plays a critical role in shifting the phase boundary between discs and vesicles, toward higher temperatures. This observation is in good agreement with lipid mixtures containing a higher molar ratio of charged lipids (Figure 1a).

Low-T Incubation. Figure 5 contains SANS data from the C_{lp} = 0.3%, R = 0.001 sample at 10 °C after more than 20 h of incubation at 4 °C. The SANS pattern contains oscillations completely different from that of a freshly prepared sample (as was described in the previous section). The data from the incubated sample is well fit using a single spherical shell model (Supporting Information section III), where the shell and the enclosed core are assumed to have the SLDs of lipid and D_2O,

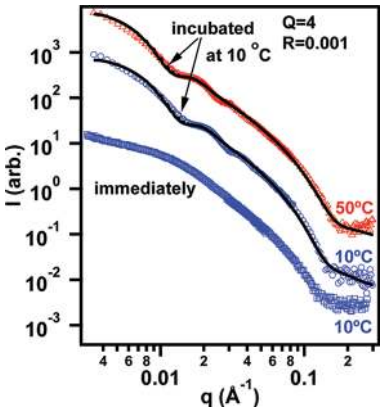

Figure 5. SANS data of R = 0.001 (no salt) samples step-diluted from 10% to 0.2% (squares) and 0.3% (circles) at 4 °C. Data for the 0.2% sample were obtained within 3 h (same as the red squares in Figure 4) after sample preparation, while data for the 0.3% sample were taken after incubation at 4 °C for >20 h. The 0.3% incubated sample then was heated to 50 °C (triangles). Data for the incubated sample were fitted using the spherical shell model.

indicative of ULVs. The best fit result yields low polydispersity (p = 25%) ULVs with an average inner radius, $\langle R_i \rangle$, of 164 ± 9 Å and a shell thickness of 37 ± 3 Å (Table 1). This morphology is in sharp contrast to the above-mentioned discs and elongated ribbon structures that are formed immediately after preparation at 10 °C (Figure 4). Moreover, the ULV structure persists as the temperature is elevated to 50 °C, instead of transforming into thermodynamically stable MLVs (as mentioned in the High-T Dilution section), indicating that these ULVs are kinetically trapped. Another interesting observation arising from these kinetically trapped ULVs is that these best fit to the high-T data results in larger $\langle R_i \rangle$ (194 ± 15 Å) and thinner shell (i.e., bilayer, 32 ± 3 Å) ULVs, as shown in Table 1. The thinner bilayer is expected as DMPC is in the L_α phase ($T_M \approx$ 23 °C for pure DMPC) at 50 °C, while a larger $\langle R_i \rangle$ can be explained in terms of uneven, crumpled gel-phase ULVs (low-T) being smoothed out at high-T, a notion consistent with a recent cryo-TEM study of dipalmitoyl phosphatidylcholine (DPPC) ULVs.[70] Similar crumpled membranes have been found in partially polymerized lipid vesicles, a result possibly due to the lipid's inherent chirality and the tilting of its hydrocarbon chains.[71] It seems, however, that this irregular topology can be annealed away, at least in the case of DPPC vesicles, when they undergo the gel-to-liquid crystalline transition. If the same crumpling phenomenon takes place in DMPC/DHPC ULVs, smaller ULVs are then expected to form at low-T—given the same amount of material (i.e., less effective area).

DISCUSSION

Although low-T ULVs have been previously observed in similar systems,[46,72] their mechanism of formation is not well understood. The observations made here pose two fundamental questions: (1) are all low-T discoidal micelles thermodynamically unstable—even though they are consistently reproduced? (2) Which physical parameter controls the rate of formation of low-T ULVs?

Stability of Discoidal Micelles. In the case of weakly charged lipid mixtures, the answer to the first question is straightforward, i.e., discoidal micelles have been shown to be unstable as demonstrated by the formation of monodisperse ULVs at low-T. However, whether or not this applies to all such systems (i.e., including strongly charged systems) remains presently unknown and will be the topic of future research. For example, a time-resolved study tracking the growth/transformation of nanodiscs will most likely be able to address this issue. Since the current study shows that charge density is one of the key parameters controlling the disc's folding process, monitoring the change in disc diameter as a function of charge density (at constant T) may reveal how the aggregate structure evolves with time. In the case of thermodynamically stable nanodiscs, their radius may grow initially after dilution, but should stabilize after equilibration.

Parameters Controlling the Formation of Low-T ULVs. With regard to which physical parameter controls the formation of these low-T ULVs, several models have been proposed to explain the spontaneous formation mechanism of ULVs associated with the line tension present at the disc's edge.[47,49,73] These models invoke a growth stage that is triggered by insufficient amounts of the short-chain lipid (i.e., DHPC). This is because, with increased temperature or decreased C_{lp}, DHPC's solubility in water and its miscibility with DMPC increase. The discs thus gradually increase in size through coalescence with neighboring discs in order to reduce the increased line tension that comes about from exposing hydrophobic chains to water. Nanodiscs grow up to a certain size, whereupon they begin to self-fold into ULVs. The disc's self-folding process includes two essential components: (1) there is a continuous loss of the DHPC that coats the disc's rim; and (2) the membrane is sufficiently flexible in order that it can self-fold.

1. Insufficient DHPC. The loss of DHPC coupled with C_{lp} and temperature determines the effective collision frequency, F_{eff}, that results in the growth of the discs. It should be noted that the greater the F_{eff}, the larger the discs. These larger discs are also more stable than their smaller counterparts because less "edge" lipid (i.e., DHPC) is required to stabilize them. Compared to the control sample (R = 0.01), a higher collision frequency (not necessarily F_{eff}) is expected in either weakly charged (R = 0.001) or highly charge-screened samples (R = 0.01, [NaCl] = 0.2 M) as a result of less interparticle Coulombic repulsion. Hence, larger and more stable discs would have been anticipated if there had been insufficient DHPCs coating the disc's edge. The fact that the control sample (R = 0.01) yields more stable discs (in terms of longer time and lower C_{lp}) implies that an insufficient amount of DHPC may not be the only determining factor in ULV formation.

2. Membrane Rigidity. Another possible parameter determining ULV formation is membrane rigidity. It has been reported that lipid membranes become more flexible with decreased surface charge density.[74,75] For this reason, the control sample (R = 0.01) bilayers are expected to be more rigid than those from the other two mixtures (i.e., R = 0.01, [NaCl] = 0.2 M, and R = 0.001), thus retarding, or possibly even prohibiting the transformation of discs into ULVs.

In order to further comprehend the issue of membrane rigidity and ULV formation, analysis using the first-order quasi-Bragg peak of 10% samples (Figure 3) has been conducted using Caillé theory,[76] where the structure factor $S(q)$ is described as $(q - q_o)^{-2+\eta}$. The Caillé parameter, η, is inversely proportional to $\sqrt{\kappa}$, where κ describes the membrane's rigidity. Since $S(q)$ is sitting on top of the form factor $P(q)$, which results in a local slope, values of $S(q)$ are extracted via dividing $I(q)$ by $P(q)$, which is obtained through best fits of the background around the first-order quasi-Bragg peak. Figure 6 illustrates the normalized $S(q)$

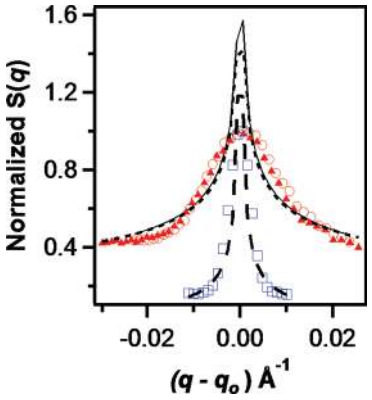

Figure 6. Normalized $S(q)$ versus $(q - q_o)$ for three 10% samples at 50 °C best fit with Caillé model: (1) $R = 0.01$ (open squares) with the best fit (dashed line); (2) $R = 0.01$, [NaCl] = 0.2 M (open circles) with the best fit (solid line); (3) $R = 0.001$ (solid triangles) with the best fit (dotted line).

[i.e., $S(q)/S(q_o)$] as a function of $(q - q_o)$, and the best fits using Caillé theory—the fits do not perfectly describe the peaks (most likely due to the inherently poor resolution of the SANS data), but provide some insight into the relative changes taking place in the membrane's rigidity. In the case of the $R = 0.01$ sample, η has a value of 1.31 and increases to 1.68 for both $R = 0.01$, [NaCl] = 0.2 M, and $R = 0.001$ samples, indicative of screened or reduced Coulombic interactions resulting in reduced membrane rigidity. Moreover, the normalized $S(q)$ of the weakly charged ($R = 0.001$) system is almost identical to that of high-salinity ([NaCl] = 0.2 M and $R = 0.001$) samples, implying that the interactions in the two membrane systems are similar. A similar trend in η has also been observed in other surfactant systems when a charged species was introduced.[77]

As a result of this analysis, we propose the following kinetics scenario for low-T ULVs found in weakly charged or high-salinity lipid mixtures. The original discoidal micelles (i.e., low-T and $C_{lp} = 10\%$) transform into elongated ribbons after dilution to a lower C_{lp}. Because of the low solubility between gel-DMPC and L_α-DHPC, the discs/ribbons are initially metastable and slowly fuse with other ribbons or discs in order to minimize rim tension, forming lamellae. Due to an inherent lower membrane rigidity—compared to relatively highly charged ($R = 0.01$) systems—the lamellae slowly self-fold into ULVs (even with DMPC in the gel phase), achieving a lower free energy state. However, highly flexible membranes (e.g., zwitterioinc mixtures) may self-fold too rapidly, forming MLVs. The fact that the initial nanodiscs are reasonably stable implies that re-equilibration (or repartition) of DMPC and DHPC within the same aggregate is most likely not responsible for the slow disc-to-vesicle kinetics—based on a lipid lateral diffusion of ~1 $\mu m^2/s$ in gel-phase bilayers.[78] In any case, these low-T ULVs are not thermodynamically stable, since the Coulombic and entropic repulsive forces are not strong enough, by themselves, to cause MLVs to unbind.

3. Other Examples. The formation mechanism of low-T, low-charge ULVs from nanodiscs, due to reduced membrane rigidity, is robust and reproducible, and can convincingly explain several cases of unstable discs at low-T and low C_{lp}. An example supporting this notion is the observation of MLVs in a zwitterionic DMPC/DHPC mixture immediately after dilution at 10 °C and $C_{lp} \leq 1\%$.[13] These neutral bilayers are presumably much more flexible, resulting in an accelerated self-folding process, that leads to the formation of MLVs. Another example is the bicellar mixture with $Q = 4$ and $R = 0.03$, where ULV size is found to be practically independent of C_{lp} and salt concentration after the samples had been incubated at 4 °C for over a period of one month.[79] In this case, ULVs might have already formed even prior to an increase in temperature (not confirmed)—this mechanism of ULV formation is most likely similar to what is taking place in the current study. Moreover, this study also shows that ULVs are most likely stable at low-T for an extended period of time (e.g., months). However, the stability of high-T ULVs was not studied here, but based on previous data,[79] we anticipate that they may also be stable for periods of weeks.[45] It should also be noted that the thermodynamic unbinding of MLVs requires a lower bending rigidity of the membrane in order to enhance steric repulsion (i.e., thermal undulation).[7] The difference between these two scenarios is mainly due to how the ULVs were formed, in the first place, i.e., thermodynamically driven or kinetically trapped. The weakly charged system ($R = 0.001$), though it forms ULVs, does not have sufficient Coulombic repulsion to unbind MLVs (Figure 3).

CONCLUSION

The present SANS study shows that MLVs obtained from high-T dilution are thermodynamically stable, in both reduced charge density and NaCl-doped systems. As these mixtures are diluted at low-T (10 °C), nanodiscs and elongated ribbons are initially observed. However, after a prolonged period of incubation (>20 h), both morphologies transform into kinetically trapped ULVs, which remain unaltered even after heating to temperatures where MLVs are commonly observed. This is good evidence that both nanodiscs and ribbons are not thermodynamically stable morphologies, even though they reproducibly form when diluted at low-T from high C_{lp} samples.

The formation mechanism of low polydispersity, kinetically trapped ULVs is fundamentally different from that of ULVs formed through the thermal unbinding of MLVs.[6,7] The present ULVs are presumably the result of a more rigid membrane that retards the self-folding of discs—a scenario unfavorable to MLV formation. However, in the case of higher charge density ($R = 0.01$) samples, discs seem to remain stable at low temperature for two reasons: (1) a reduction in the effective collision frequency; and (2) increased membrane rigidity. In other words, the mechanism that transforms nanodiscs to ULVs at low temperature is the result of a fine balance between membrane rigidity, C_{lp}, and charge density. This knowledge may prove to be useful when designing lipid-based delivery carriers for pharmaceuticals, where morphological changes are crucial in effectively delivering payloads.

Future kinetic studies on the structural evolution of discs → ULVs using time-resolved techniques are necessary in order to fully understand the key parameters controlling this transformation and eventually identifying the thermodynamically stable morphology.

ASSOCIATED CONTENT

Supporting Information. Description and calculations of models used for best fitting the SANS data. This material is available free of charge via the Internet at http://pubs.acs.org.

AUTHOR INFORMATION

Corresponding Author

*Mu-Ping Nieh, Tel: 860-486-8708; e-mail: mu-ping.nieh@ims.uconn.edu.

■ ACKNOWLEDGMENT

This work made use of facilities supported in part by the National Science Foundation under Agreement No. DMR-0944772. The mention of commercial products does not imply endorsement by NIST, nor does it imply that the materials or equipment identified are necessarily the best available for the purpose. The work at ORNL's High Flux Isotope Reactor was sponsored by the Scientific User Facilities Division, Office of Basic Energy Sciences, United States Department of Energy (U.S. DOE). ORNL is operated by UT−Battelle, LLC for the U.S. DOE under Contract No. DE-AC05-00OR22725. M.-P. N. is grateful for the funding support from University of Connecticut (UConn) faculty large grant and the startup fund provided by Institute of Materials Science (IMS) at UConn. J. K. is supported through ORNL's Laboratory Directed Research and Development (LDRD) and Program Development programs.

■ REFERENCES

(1) Hwang, K. J.; Padki, M. M.; Chow, D. D.; Essien, H. E.; Lai, J. Y.; Beaumier, P. L. *Biochim. Biophys. Acta* **1987**, *901*, 88–96.
(2) Gabizon, A.; Shmeeda, H.; Barenholz, Y. *Clin. Pharmacokinet.* **2003**, *42*, 419–436.
(3) Lipowsky, R.; Leibler, S. *Phys. Rev. Lett.* **1986**, *35*, 7004–7009.
(4) Leibler, S.; Lipowsky, R. *Phys. Rev. B* **1987**, *56*, 2541–2544.
(5) Mutz, M.; Helfrich, W. *Phys. Rev. Lett.* **1989**, *62*, 2881–2884.
(6) Milner, S. T.; Roux, D. *J. Phys. I France* **1992**, *2*, 1741–1754.
(7) Pozo-Navas, B; Raghunathan, V. A.; Katsaras, J.; Rappolt, M.; Lohner, K.; Pabst, G. *Phys. Rev. Lett.* **2003**, *91*, 028101.
(8) Pabst, G.; Katsaras, J.; Raghunathan, V. A.; Rappolt, M. *Langmuir* **2003**, *19*, 1716–1722.
(9) Gabriel, N. E.; Roberts, M. E. *Biochemistry* **1984**, *23*, 4011–4015.
(10) Gabriel, N. E.; Roberts, M. E. *Biochemistry* **1986**, *25*, 2812–2821.
(11) Hauser, H.; Gains, N.; Eibl, H.-J.; Müller, M.; Wehrli, E. *Biochemistry* **1986**, *25*, 2126–2134.
(12) Nieh, M.-P.; Glinka, C. J; Krueger, S.; Prosser, R. S.; Katsaras, J. *Langmuir* **2001**, *17*, 2629–2638.
(13) Nieh, M.-P.; Glinka, C. J; Krueger, S.; Prosser, R. S.; Katsaras, J. *Biophys. J.* **2002**, *82*, 2487–2498.
(14) Sanders, C. R., II; Prestegard, J. H. *Biophys. J.* **1990**, *58*, 447–460.
(15) Sanders, C. R., II; Prestegard, J. H. *J. Am. Chem. Soc.* **1991**, *113*, 1987–1996.
(16) Sanders, C. R., II; Schwonek, J. P. *Biochemistry* **1992**, *31*, 8898–8905.
(17) Chung, J.; Prestegard, J. H. *J. Phys. Chem.* **1993**, *97*, 9837–9843.
(18) Struppe, J.; Vold, R. R. *J. Magn. Reson.* **1998**, *135*, 541–546.
(19) Sanders, C. R., II; Prosser, C. R. *Structure* **1998**, *6*, 1227–1234.
(20) Picard, F.; Paquet, M.-J.; Levesque, J.; Bélanger, A.; Auger, M. *Biophys. J.* **1999**, *77*, 888–902.
(21) Raffard, G.; Steinbrukner, S.; Arnold, A.; Davis, J. H.; Dufourc, E. J. *Langmuir* **2000**, *16*, 7655–7662.
(22) Struppe, J.; Vold, R. R. *J. Magn. Reson.* **1998**, *135*, 541–546.
(23) Tiburu, E. K.; Moton, D. M.; Logan, G. A. *Biochim. Biophys. Acta* **2001**, *1512*, 206–214.
(24) Sternin, E.; Nizza, D.; Gawrisch, K. *Langmuir* **2001**, *17*, 2610–2616.
(25) Arnold, A.; Labrot, T.; Oda, R.; Dufourc, E. J. *Biophys. J.* **2002**, *83*, 2667–2680.
(26) Rowe, B. A.; Neal, S. L. *Langmuir* **2003**, *19*, 2039–2048.
(27) van Dam, L.; Karlsson, G.; Edwards, K. *Biochim. Biophys. Acta* **2004**, *1664*, 241–256.
(28) Katsaras, J.; Harroun, T. A.; Pencer, J.; Nieh, M.-P. *Naturwissenschaften* **2005**, *92*, 355–366.
(29) Soong, R.; Nieh, M.-P.; Nicholson, E.; Katsaras, J.; Macdonald, P. M. *Langmuir* **2010**, *26*, 2630–2638.
(30) Triba, M. N.; Warschawski, D. E.; Devaux, P. F. *Biophys. J.* **2005**, *88*, 1887–1901.
(31) Howard, K. P.; Opella, S. J. *J. Magn. Reson.* **1996**, *112*, 91–94.
(32) Tjandra, N.; Bax, A. J. *Science* **1997**, *278*, 1111–1114.
(33) Marassi, F. M.; Ramamoorthy, A.; Opella, S. J. *Proc. Natl. Acad. Sci.* **1997**, *94*, 8551–8556.
(34) Vold, R. R.; Prosser, R. S.; Deese, A. J. *J. Biomol. NMR* **1997**, *9*, 329–335.
(35) Losonczi, J. A.; Prestegard, J. H. *J. Biomol. NMR* **1998**, *12*, 447–451.
(36) Glover, K. J.; Whiles, J. A.; Wu, G.; Yu, N.; Deems, R.; Struppe, J. O.; Stark, R. E.; Komives, E. A.; Vold, R. R. *Biophys. J.* **2001**, *81*, 2163–2171.
(37) Opella, S. J.; Nevzorov, A.; Mesieh, M. F.; Marassi, F. M. *Biochem. Cell Biol.* **2002**, *80*, 597–604.
(38) Whiles, J. A.; Deems, R.; Vold, R. R.; Dennis, E. A. *Bioorg. Chem.* **2002**, *30*, 431–442.
(39) Zandomeneghi, G.; Williamson, P. T. F.; Hunkeler, A.; Meier, B. H. *J. Biomol. NMR* **2003**, *25*, 125–132.
(40) Marcotte, I.; Dufourc, E. J.; Ouellet, M.; Auger, M. *Biophys. J.* **2003**, *85*, 328–339.
(41) Li, X.; Goodson, B. M. *Langmuir* **2004**, *20*, 8437–8441.
(42) Marcotte, I.; Auger, M. *Concepts Magn. Reson. Part A* **2005**, *24*, 17–35.
(43) Prosser, R. S.; Evanics, F.; Kitevski, J. L.; Al-Abdul-Wahid, M. S. *Biochemistry* **2006**, *45*, 8453–8465.
(44) Diller, A.; Loudet, C.; Aussenac, F.; Raffard, G.; Fournier, S.; Laguerre, M.; Grélard, A.; Opella, S. J.; Marassi, F. M.; Dufourc, E. J. *Biochimie* **2009**, *91*, 744–751.
(45) Nieh, M.-P.; Harroun, T. A.; Raghunathan, V. A.; Glinka, C. J.; Katsaras, J. *Phys. Rev. Lett.* **2003**, *91*, 158105.
(46) Nieh, M.-P.; Harroun, T. A.; Raghunathan, V. A.; Glinka, C. J.; Katsaras, J. *Biophys. J.* **2004**, *86*, 2615–2629.
(47) Nieh, M.-P.; Kučerka, N.; Katsaras, J. *Methods Enzymol.* **2009**, *465*, 3–20.
(48) Nieh, M.-P.; Raghunathan, V. A.; Kline, S. R.; Harroun, T. A.; Huang, C.-Y.; Pencer, J.; Katsaras, J. *Langmuir* **2005**, *21*, 6656–6661.
(49) Leng, J.; Egelhaaf, S. U.; Cates, M. E. *Biophys. J.* **2003**, *85*, 16214–1646.
(50) Egelhaaf, S. U.; Schurtenberger, P. *Phys. Rev. Lett.* **1999**, *82*, 2804–2807.
(51) Glinka, C. J.; Barker, J. G.; Hammouda, B.; Krueger, S.; Moyer, J. J.; Orts, W. J. *J. Appl. Crystallogr.* **1998**, *31*, 430–445.
(52) Mildner, D. F. R.; Carpenter, J. M.; Worcester, D. L. *J. Appl. Crystallogr.* **1986**, *19*, 311–319.
(53) Kline, S. R. *J. Appl. Crystallogr.* **2006**, *39*, 895–900.
(54) van Dam, L.; Karlsson, G.; Edwards, K. *Langmuir* **2006**, *22*, 3280–3285.
(55) Higgins, J. S.; Benoit, H. C. *Polymers and Neutron Scattering*; Oxford University Press: New York, 1994; Chapter 6.
(56) Vinson, P. K.; Talmon, Y.; Walter, A. *Biophys. J.* **1989**, *56*, 669–681.
(57) Chiruvolu, S.; Warriner, H. E.; Naranjo, E.; Idziak, S. H. J.; Rädler, J. O.; Plano, R. J.; Zasadzinski, J. A.; Safinya, C. R. *Science* **1994**, *266*, 1222–1225.
(58) Hui, S. W.; He, N.-B. *Biochemistry* **1983**, *22*, 1159–1164.
(59) Caffrey, M.; Hogan, J.; Mencke, A. *Biophys. J.* **1991**, *31*, 8898–8905.
(60) Kiselev, M. A.; Lombardo, D.; Leiseur, P.; Kisselev, A. M.; Borbely, S.; Simonova, T. N.; Barsukov, L. I. *Chem. Phys.* **2008**, *345*, 173–180.
(61) Carmona-Ribeiro, A. M. *Curr. Med. Chem.* **2006**, *13*, 1359–1370.
(62) Vinson, P. K.; Bellare, J. R.; Davis, H. T.; Miller, W. G.; SCriven, L. E. *J. Colloid Interface Sci.* **1991**, *142*, 74–91.
(63) Bayburt, T. H.; Grinkova, Y. V.; Sligar, S. G. *Nano Lett.* **2002**, *2*, 853–856.
(64) Shaw, A. W.; McLean, M. A.; Sligar, S. G. *FEBS Lett.* **2004**, *556*, 260–264.
(65) Denisov, I. G.; Grinkova, Y. V.; Lazarides, A. A.; Sligar, S. G. *J. Am. Chem. Soc.* **2004**, *126*, 3477–3487.

(66) Richie, T. K.; Grinkova, Y. V.; Bayburt, T. H.; Denisov, I. G.; Zolnerciks, J. K.; Atkins, W. M.; Sligar, S. G. *Methods Enzymol.* **2009**, *464*, 211–231.
(67) Bayburt, T. H.; Sligar, S. G. *FEBS Lett.* **2010**, *584*, 1721–1727.
(68) Sasaki, R.; Sasaki, H.; Fukuzawa, S.; Kikuchi, J.; Hirota, H.; Tachibana, K. *Bull. Chem. Soc. Jpn.* **2007**, *80*, 1208–1216.
(69) Tristram-Nagle, S.; Liu, Y.; Legleiter, J.; Nagle, J. F. *Biophys. J.* **2002**, *83*, 3324–3335.
(70) Hirst, L.; Ossowski, A.; Fraser, M. *American Physical Society (March Meeting)*, Dallas, TX, 2011.
(71) Chaieb, S.; Natrajan, V. K.; El-rahman, A. A. *Phys. Rev. Lett.* **2006**, *96*, 078101.
(72) Mahabir, S.; Wan, W. K.; Katsaras, J.; Nieh, M.-P. *J. Phys. Chem. B* **2010**, *114*, 5729–5735.
(73) Fromherz, P *Chem. Phys. Lett.* **1983**, *94*, 259–266.
(74) Higgs, P. G.; Joanny, J.-F. *J. Phys. (France)* **1990**, *51*, 2307–2320.
(75) Claessens, M. M. A. E.; van Oort, B. F.; Leermakers, F. A. M.; Hoekstra, F. A.; Cohen Stuart, M. A. *Biophys. J.* **2004**, *87*, 3882–3892.
(76) Caillé, A. *C. R. Acad. Sci. Paris, B* **1972**, *274*, 891–893.
(77) Safinya, C. R.; Sirota, E. B.; Roux, D.; Smith, G. S. *Phys. Rev. Lett.* **1989**, *62*, 1134–1137.
(78) Fostner, M. B.; Yee, C. K.; Parikh, A. N.; Groves, J. T. *J. Am. Chem. Soc.* **2006**, *128*, 15221–15227.
(79) Yue, B.; Huang, C.-Y.; Nieh, M.-P.; Glinka, C. J.; Katsaras, J. *J. Phys. Chem. B* **2005**, *109*, 609–616.